Electronic Supplementary Material (ESI) for Dalton Transactions.
This journal is © The Royal Society of Chemistry 2017

Key-role of composition and structural features on fluoride ion conductivity in tysonite $Ce_{1-x}Sr_xF_{3-x}$ solid solutions

Belto Dieudonné, Johann Chable, Monique Body, Christophe Legein, Etienne Durand, Fabrice Mauvy, Sébastien Fourcade, Marc Leblanc, Vincent Maisonneuve, and Alain Demourgues

Electronic Supporting Information

Fig. S1. Powder XRD Rietveld refinement of CeF_3. 2
Fig. S2. Powder XRD Rietveld refinement of $Ce_{0.99}Sr_{0.01}F_{2.99}$. 2
Fig. S3. Powder XRD Rietveld refinement of $Ce_{0.95}Sr_{0.05}F_{2.95}$. 3
Fig. S4. Powder XRD Rietveld refinement of $Ce_{0.93}Sr_{0.07}F_{2.93}$. 3
Fig. S5. Powder XRD Rietveld refinement of $Ce_{0.90}Sr_{0.10}F_{2.90}$. 4
Table S1. Unit cell parameters (Å) and volume (Å^3) of $Ce_{1-x}Sr_xF_{3-x}$ 4
Table S2. F–(Ce,Sr) distances (Å) in $Ce_{1-x}Sr_xF_{3-x}$. 5
Fig. S6. ^{19}F MAS NMR spectra of CeF_3 recorded at 64 kHz and 54 kHz 6
Fig. S7. Experimental and fitted ^{19}F MAS (64 kHz) NMR spectra of $Ce_{0.975}Sr_{0.025}F_{2.975}$ 7
Table S3. Isotropic chemical shift, chemical shift anisotropy, asymmetry parameter of the CSA tensor, linewidth, relative intensity and assignment of the NMR resonances used for the fit of the ^{19}F MAS (64 kHz) NMR spectrum of $Ce_{0.975}Sr_{0.025}F_{2.975}$ 7
Fig. S8. Experimental and fitted ^{19}F MAS (64 kHz) NMR spectra of $Ce_{0.95}Sr_{0.05}F_{2.95}$. 8
Table S4. Isotropic chemical shift, chemical shift anisotropy, asymmetry parameter of the CSA tensor, linewidth, relative intensity and assignment of the NMR resonances used for the fit of the ^{19}F MAS (64 kHz) NMR spectrum of $Ce_{0.95}Sr_{0.05}F_{2.95}$. 8
Table S5. Relative intensities of the ^{19}F NMR resonances assigned to F1 and F2,3, expected from formulation considering fluorine vacancies on F1 site and estimated from the fits of the NMR spectra recorded at 64°C and fractions of mobile F2 and F3 atoms in $Ce_{1-x}Sr_xF_{3-x}$ compounds 9
Fig. S9. ^{19}F MAS NMR spectra of $Ce_{0.99}Sr_{0.01}F_{2.99}$ recorded at 64 kHz and 54 kHz 10
Fig. S10. ^{19}F MAS NMR spectra of $Ce_{0.975}Sr_{0.025}F_{2.975}$ recorded at 64 kHz and 54 kHz 10
Fig. S11. Nyquist diagram obtained at 25 °C for a sintered pellet of $Ce_{0.975}Sr_{0.025}F_{2.975}$. 11

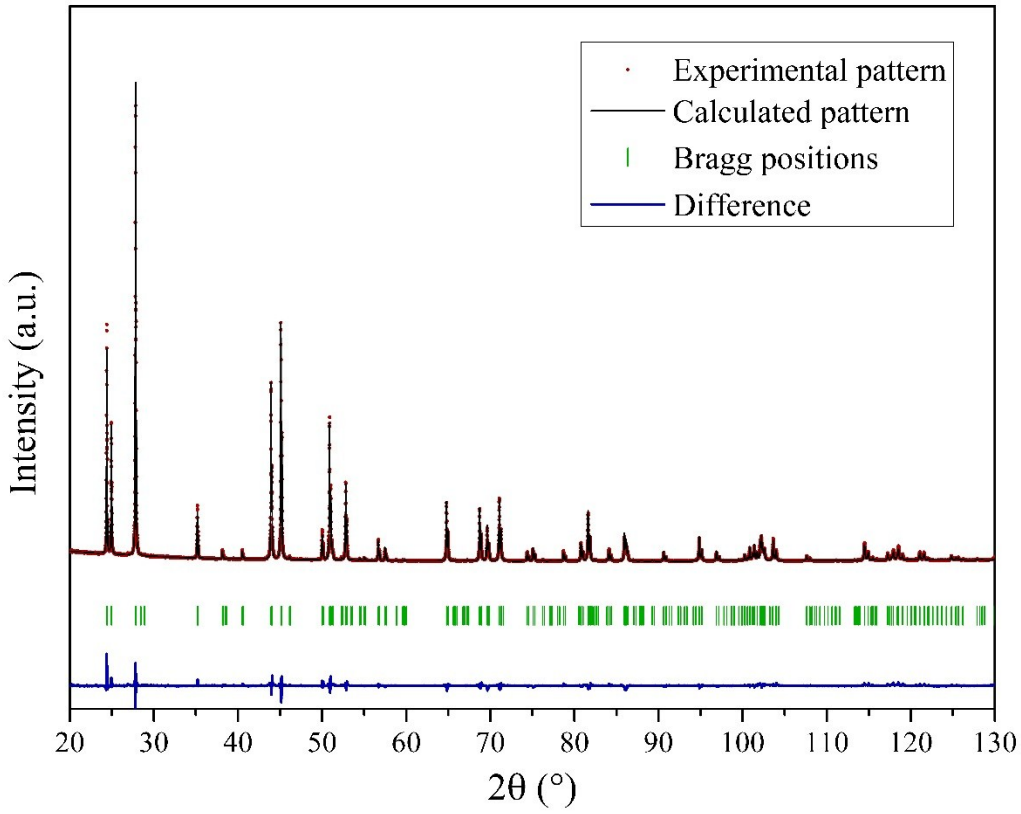

Fig. S1. Powder XRD Rietveld refinement of CeF_3.

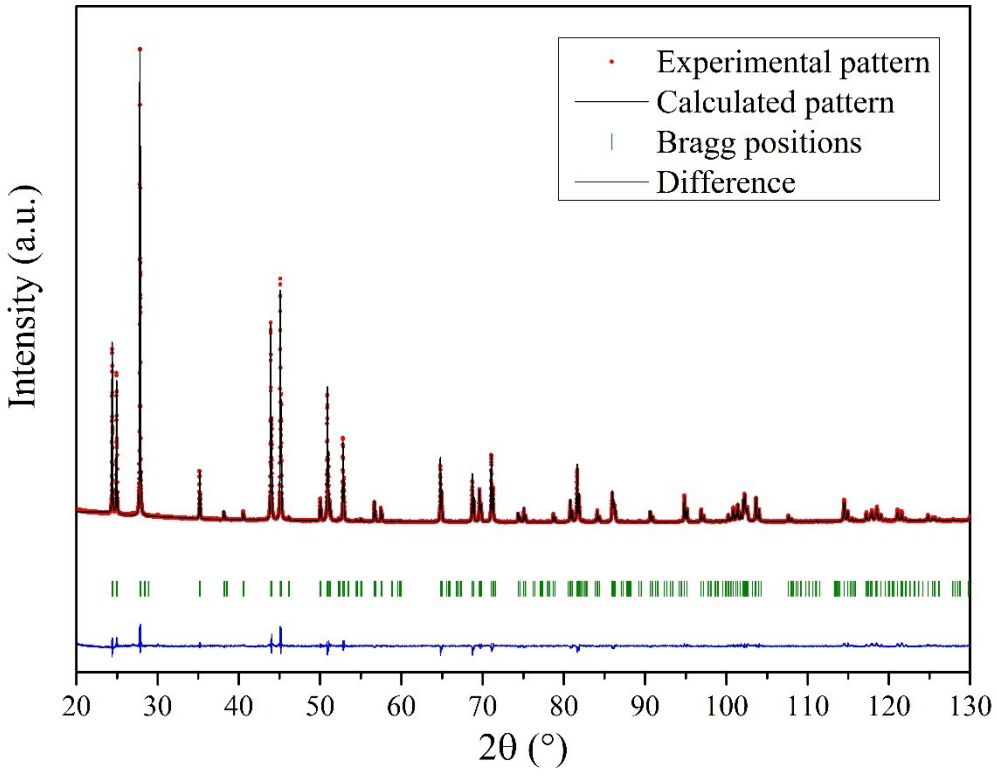

Fig. S2. Powder XRD Rietveld refinement of $Ce_{0.99}Sr_{0.01}F_{2.99}$.

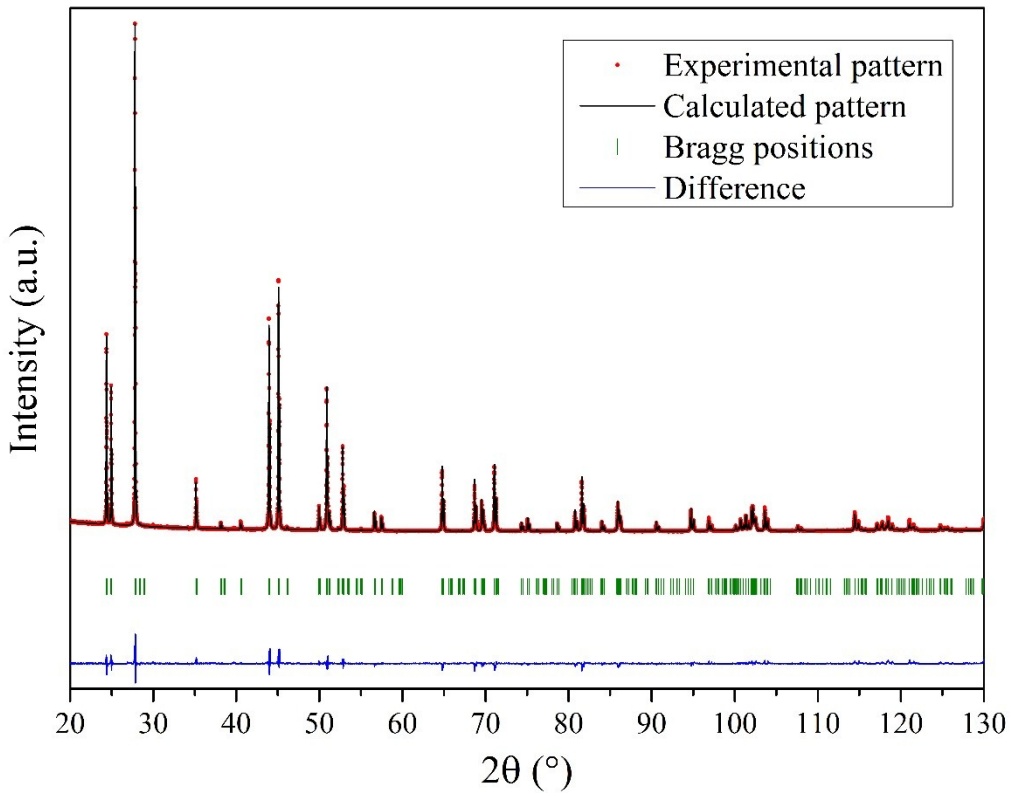

Fig. S3. Powder XRD Rietveld refinement of $Ce_{0.95}Sr_{0.05}F_{2.95}$.

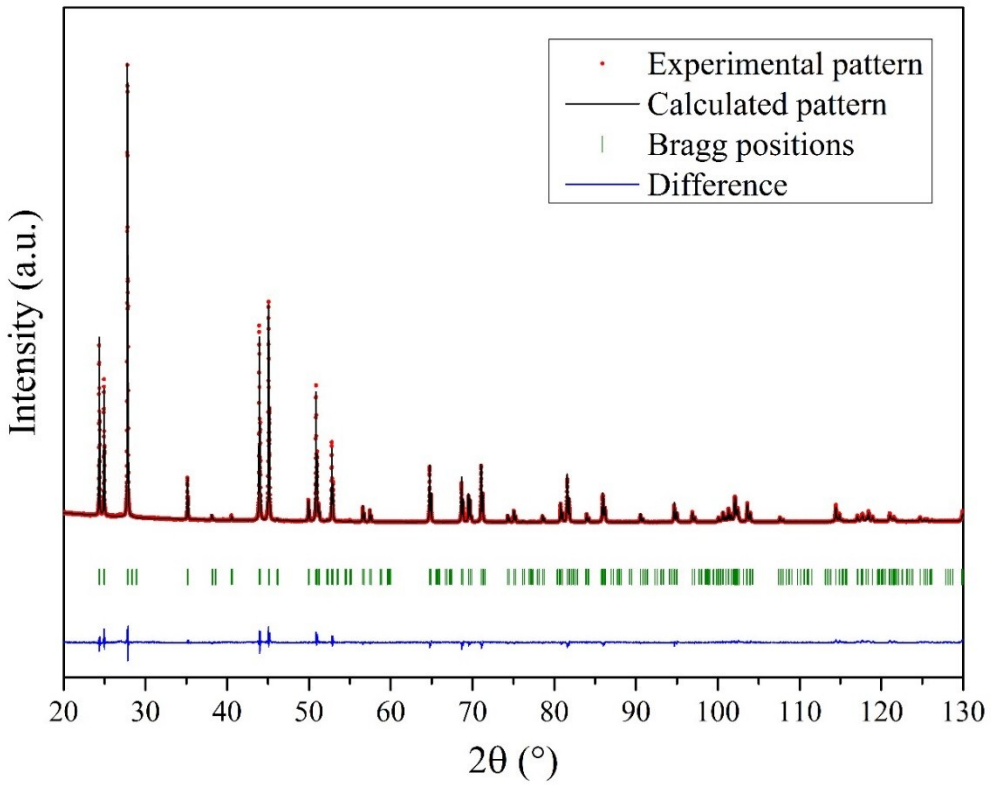

Fig. S4. Powder XRD Rietveld refinement of $Ce_{0.93}Sr_{0.07}F_{2.93}$.

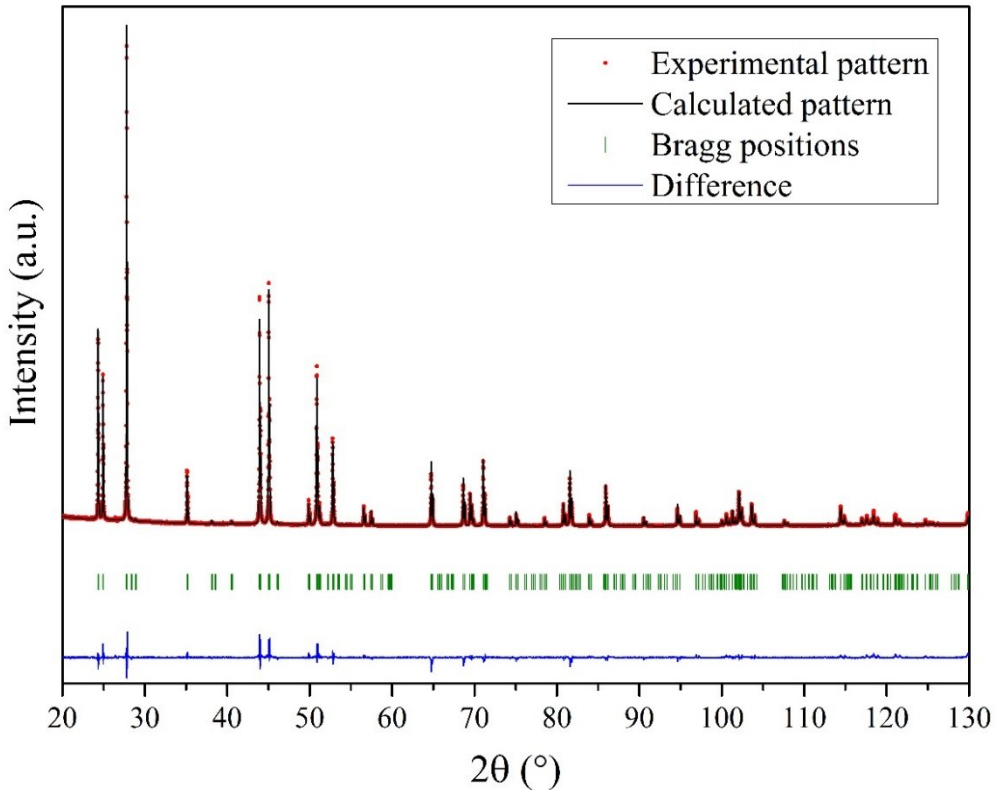

Fig. S5. Powder XRD Rietveld refinement of $Ce_{0.90}Sr_{0.10}F_{2.90}$.

Table S1. Unit cell parameters (Å) and volume (Å^3) of $Ce_{1-x}Sr_xF_{3-x}$.

x	a	c	v
0	7.1298(1)	7.2859(1)	320.76(1)
0.01	7.1300(1)	7.2870(1)	320.83(1)
0.025	7.1305(1)	7.2903(1)	321.01(1)
0.05	7.1310(1)	7.2946(2)	321.24(1)
0.07	7.1307(1)	7.2980(1)	321.36(1)
0.10	7.1300 (1)	7.3023(1)	321.50(1)

Table S2. F–(Ce,Sr) distances (Å) in $Ce_{1-x}Sr_xF_{3-x}$.

x	F1–(Ce,Sr)	<F1–(Ce,Sr)>	F2–(Ce,Sr) (x3)	F3–(Ce,Sr) (x3)
0	2.417(3) 2.452(4) 2.643(7) 3.012(5)	2.631	2.395(5)	2.430(1)
0.01	2.410(3) 2.475(4) 2.636(6) 2.994(4)	2.629	2.432(2)	2.424(1)
0.025	2.407(3) 2.471(5) 2.756(9) 2.902(5)	2.627	2.465(2)	2.329(1)
0.05	2.413(2) 2.445(5) 2.708(7) 2.955(5)	2.631	2.435(2)	2.360(1)
0.07	2.427(2) 2.460(5) 2.691(9) 2.929(6)	2.626	2.430(3)	2.429(3)
0.10	2.446(3) 2.473(13) 2.634(8) 2.922(11)	2.618	2.429(3)	2.377(1)

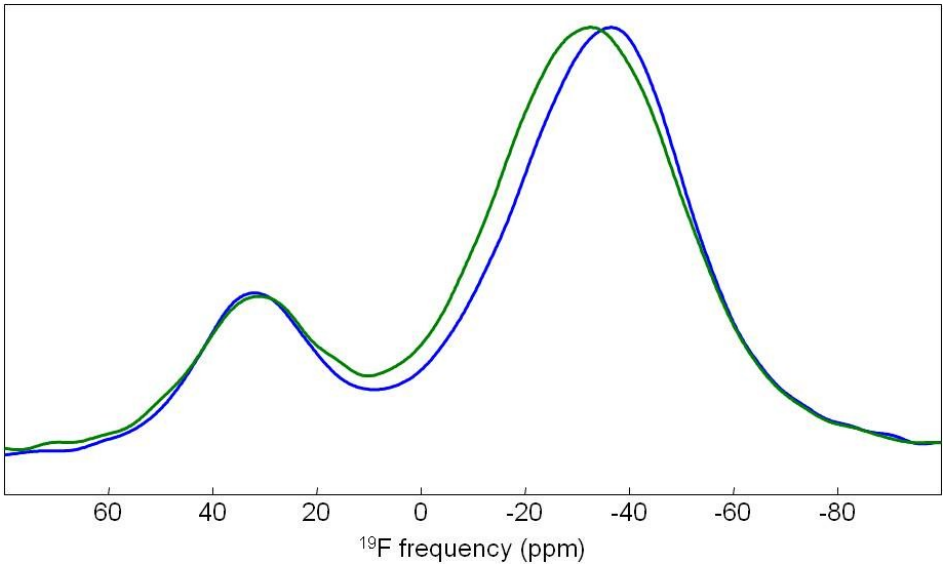

Fig. S6. ^{19}F MAS NMR spectra of CeF_3 recorded at 64 kHz (64°C, in blue) and 54 kHz (51°C, in green).

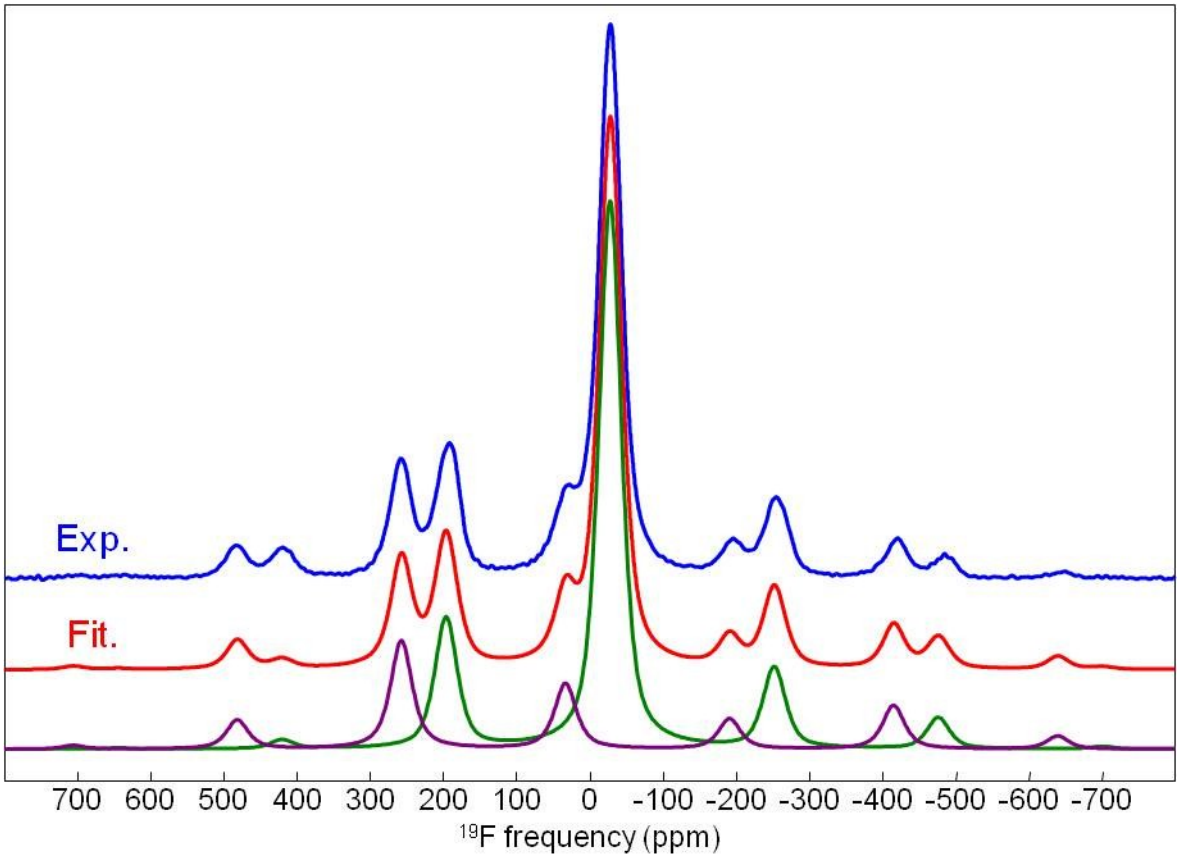

Fig. S7. Experimental and fitted ^{19}F MAS (64 kHz) NMR spectra of $Ce_{0.975}Sr_{0.025}F_{2.975}$. The individual resonances used for the fit are shown below.

Table S3. Isotropic chemical shift (δ_{iso}, ppm), chemical shift anisotropy (δ_{csa}, ppm), asymmetry parameter of the CSA tensor (η_{csa}), linewidth (LW, ppm), relative intensity (I, %) and assignment of the NMR resonances used for the fit of the ^{19}F MAS (64 kHz) NMR spectrum of $Ce_{0.975}Sr_{0.025}F_{2.975}$.

δ_{iso}	δ_{csa}	η_{csa}	LW	I	Assignment
-27.8	-359	0	36.5	72.7	F1
33.3	-763	0	35.5	27.3	F2 and F3

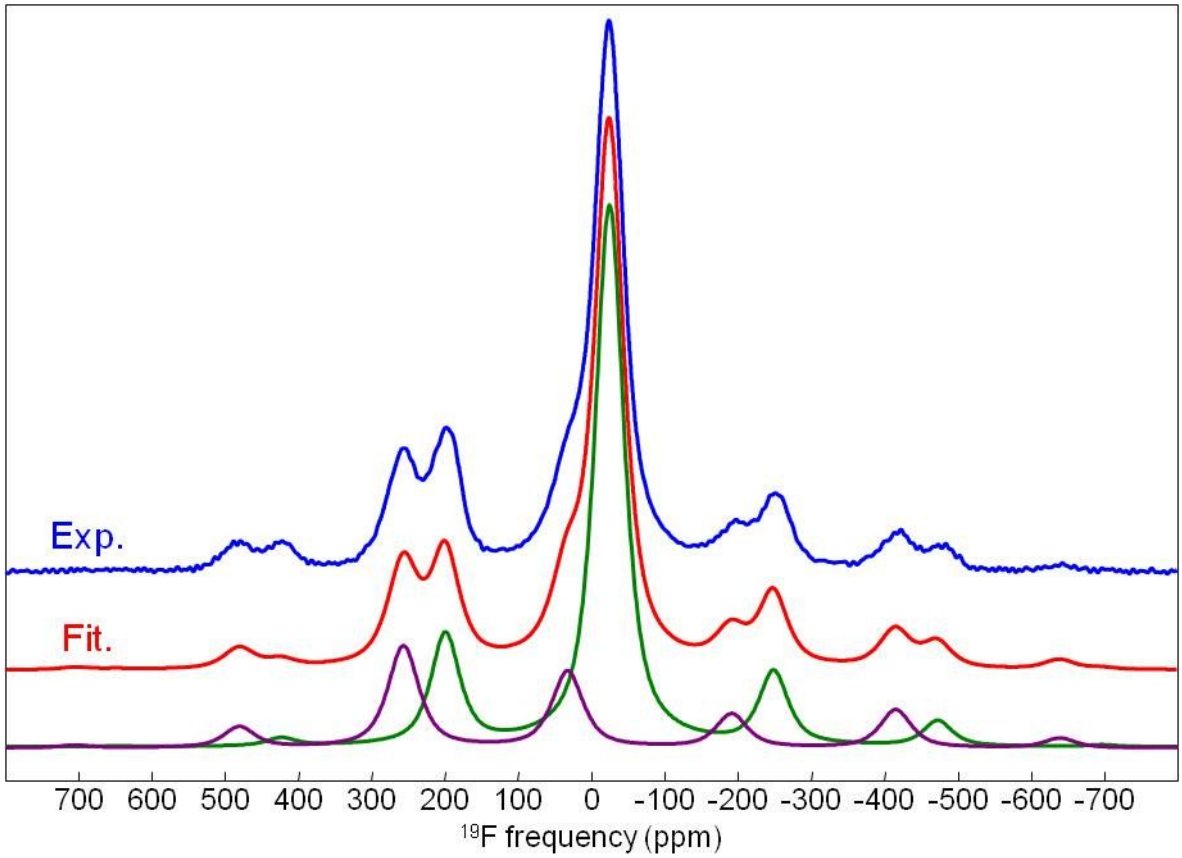

Fig. S8. Experimental and fitted ^{19}F MAS (64 kHz) NMR spectra of $Ce_{0.95}Sr_{0.05}F_{2.95}$. The individual resonances used for the fit are shown below.

Table S4. Isotropic chemical shift (δ_{iso}, ppm), chemical shift anisotropy (δ_{csa}, ppm), asymmetry parameter of the CSA tensor (η_{csa}), linewidth (LW, ppm), relative intensity (I, %) and assignment of the NMR resonances used for the fit of the ^{19}F MAS (64 kHz) NMR spectrum of $Ce_{0.95}Sr_{0.05}F_{2.95}$.

δ_{iso}	δ_{csa}	η_{csa}	LW	I	Assignment
-24.2	-336	0.2	47.1	71.7	F1
33.1	-695	0	50.5	28.3	F2 and F3

Table S5. Relative intensities (I, %) of the ^{19}F NMR resonances assigned to F1 and F2,3, expected from formulation considering fluorine vacancies on F1 site and estimated from the fits of the NMR spectra recorded at 64°C and fractions of mobile F2 and F3 atoms (%) calculated as ($\frac{I_{expected} - I_{estimated}}{I_{expected}}$) in $Ce_{1-x}Sr_xF_{3-x}$ compounds.

x	0.01		0.025		0.05	
	F1	F2,3	F1	F2,3	F1	F2,3
Expected I	66.6	33.4	66.4	33.6	66.1	33.9
Estimated I	73.9	26.1	72.7	27.3	71.7	28.3
Mobile F2 and F3 atoms	22		19		17	

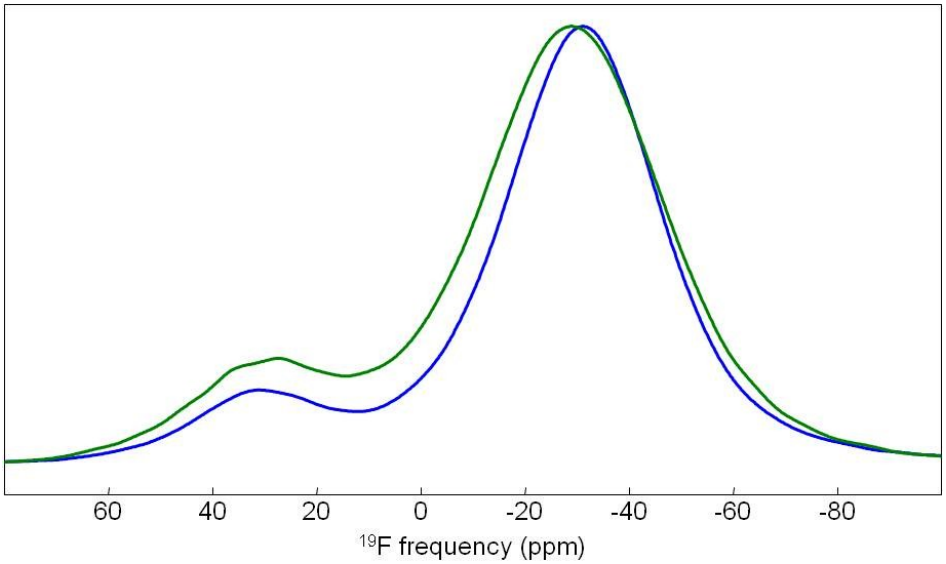

Fig. S9. ^{19}F MAS NMR spectra of $Ce_{0.99}Sr_{0.01}F_{2.99}$ recorded at 64 kHz (64°C, in blue) and 54 kHz (51°C, in green).

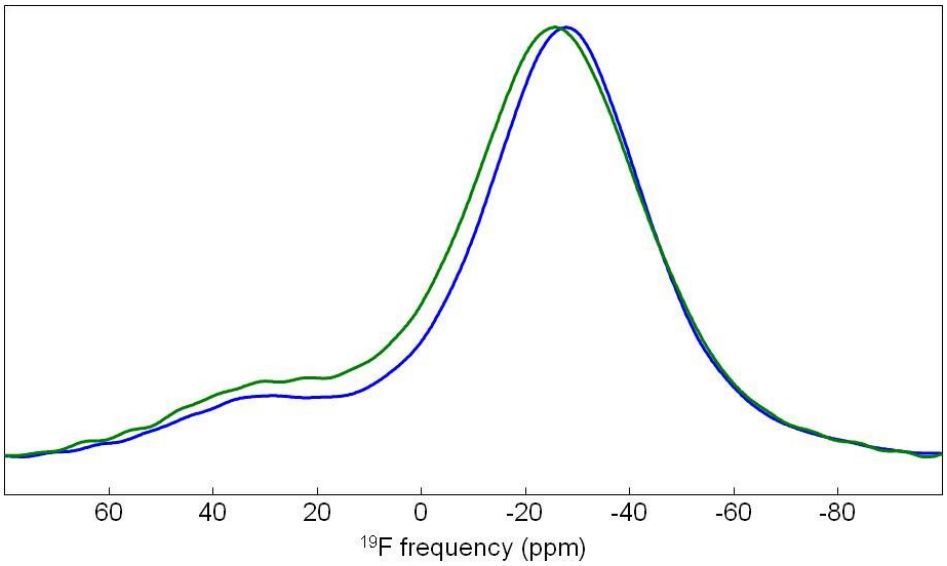

Fig. S10. ^{19}F MAS NMR spectra of $Ce_{0.975}Sr_{0.025}F_{2.975}$ recorded at 64 kHz (64°C, in blue) and 54 kHz (51°C, in green).

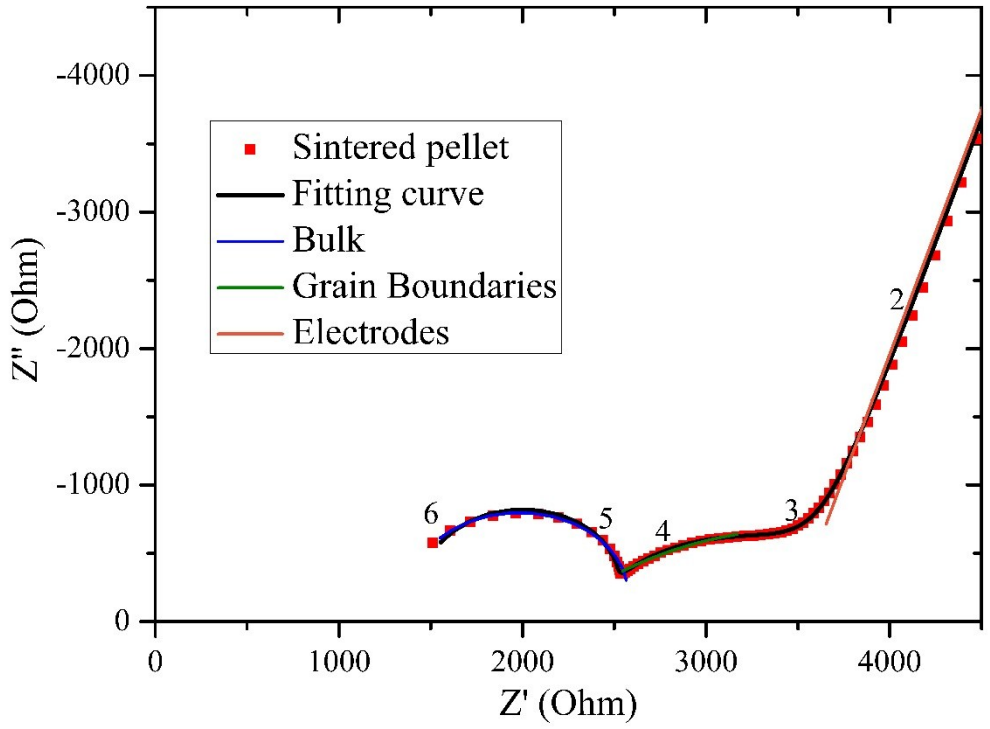

Fig. S11. Nyquist diagram obtained at 25 °C for a sintered pellet of $Ce_{0.975}Sr_{0.025}F_{2.975}$. Numbers indicate the log of the measurement frequency (e.g. 5 ⇔ 10^5 Hz).